

# Enhancement of luminous efficacy for light-emitting diodes lamps by adding $\text{CaSr}_2(\text{PO}_4)_2:\text{Eu}^{3+}$ phosphor

Ho Minh Trung<sup>1</sup>, My Hanh Nguyen Thi<sup>2</sup>

<sup>1</sup>Faculty of Basic Sciences, Vinh Long University of Technology Education, Vinh Long, Vietnam

<sup>2</sup>Faculty of Mechanical Engineering, Industrial University of Ho Chi Minh City, Ho Chi Minh City, Vietnam

## Article Info

### Article history:

Received Oct 29, 2022

Revised Jun 3, 2023

Accepted Jun 5, 2023

### Keywords:

$\text{CaSr}_2(\text{PO}_4)_2:\text{Eu}^{3+}$

CIE hue coordinates

Light-emitting diode lamps

Luminous efficacy

X-Ray diffraction

## ABSTRACT

Through employing the fluid ignition technique, we created the samples  $\text{CaSr}_2(\text{PO}_4)_2:\text{Eu}^{3+}$  with  $\text{Eu}^{3+}$  incorporated then assessed them in the form of contactless optical heat measurement as well as solid-state illumination. We identified the attributes for these samples including X-ray diffraction (XRD), photoluminescent spectroscopy, Fourier transform infrared spectroscopy (FTIS) along with photoluminescent spectroscopy correlating with temperature. XRD, along with FTIS, validates that the one-stage samples were formed via the orthophosphate anion  $(\text{PO}_4)^{3-}$ . In the case of these samples, n-UV recreation under 395 nm generated potent, orange-red discharge lines under 592 nm as well as 615 nm, which is consistent with the standard shifts between 5D0 and 7F1 as well as 5D0 and 7F2 for the  $\text{Eu}^{3+}$  ions. The International Commission on Illumination (CIE) coordinates (0.65, 0.35) based on the hue scale validate the red discharge. For the task of attaining optical heat measurement, we took advantage of the fluorescent intenseness proportion technique that utilizes heat-incorporated discharge states of 5D1 as well as 5D0 for  $\text{Eu}^{3+}$ . The samples have maximum responsiveness reaching roughly 0.0023 K<sup>-1</sup> under 323 K or small heat levels. According to the outcomes, it is possible to utilize the samples when it comes to contactless optical heat measurement as well as solid-state illumination.

*This is an open access article under the [CC BY-SA](https://creativecommons.org/licenses/by-sa/4.0/) license.*



## Corresponding Author:

My Hanh Nguyen Thi

Faculty of Mechanical Engineering, Industrial University of Ho Chi Minh City

No. 12 Nguyen Van Bao Street, Ho Chi Minh City, Vietnam

Email: nguyenthimyhanh@iuh.edu.vn

## 1. INTRODUCTION

The modern industries such as those of the optical field have become concerned about conserving natural materials due to deficiency issues and hence the need to look into devices requiring substantial power without yielding significant benefits [1], [2]. Unlike incandescent light, solid-state illumination may help us conserve power at 80% level and limit harmful discharges as well including  $\text{CO}_2$  or  $\text{SO}_2$ . The short for white-light-emitting diode (WLED) devices are held in high regard since they possess desirable qualities including small magnitude, great performance [3], greater durability, low power requirement, as well as better safety [4]. The construction of WLED devices would involve certain typical techniques employing various luminescent substances. It is possible to subject the yellow phosphor  $\text{YAG}:\text{Ce}^{3+}$  to excitation, yielding lesser short for color rendering index (CRI) along with significant short for correlated color temperature (CCT) [5]. These results are caused by insufficient red discharge. Alternative, we can create a merger between phosphors of red, green, blue and one n-UV LED chip for greater CRI as well as CCT [6], [7]. If the goal is to generate desirable white ray, red phosphors would be required. Among rare-earth ions,  $\text{Eu}^{3+}$ , which generates red ray, is usually employed. Beside reliable discharge hue, phosphor samples incorporated with  $\text{Eu}^{3+}$  offer better safety and do not require complicated

creation process [8]–[10]. As such, these samples are commonly studied.  $\text{Eu}^{3+}$  generates one thin line red orange discharge correlating with the distinct shift between  ${}^5\text{D}_0$  and  ${}^7\text{F}_j$  with J values of 1, 2, 3 and 4. The electric dipole shift generates discharges between 610 nm and 630 nm and would be commonly employed when it comes to hue exhibition as well as interior illumination. For the phosphor base's matrix, orthophosphate blends would be desirable bases as they have wide bandgap, greater chemical reliability, small heat-level requirement for creation process along with the possibility for tetrahedral  $\text{PO}_4^{3-}$  anion being binded to other formational factors [11]. Subsequently, various studies thoroughly focused on said blends to determine possible practical uses that concern gamma-radioactivity trackers, LED devices, optical heat level observation, and so on. The study herein concern utilizing these phosphor samples in contactless optical heat detectors. These detectors prove to be in high demand since they have better precision, immediate reactivity, as well as superior resolution [12]. These qualities help track heat level inside conditions with harsh heat as well as entities with rapid movement. If we modify the extrinsic heat level near the samples, electrons could occupy or leave the power states nearby with disparity between  $200\text{ cm}^{-1}$  and  $2000\text{ cm}^{-1}$ . The occupants for highest as well as lowest heat-incorporated discharge states [ $\text{Eu}^{3+}: {}^5\text{D}_1/{}^5\text{D}_0$ ] may vary based on the heat level, leading to different fluorescent intenseness proportion based on heal level disparity. Studies focused on different three-valence lanthanide ions ( $\text{Sm}^{3+}$ ,  $\text{Nd}^{3+}$ ,  $\text{Pr}^{3+}$ ,  $\text{Tb}^{3+}$ , and  $\text{Er}^{3+}$ ) to assess ability to detect optical heat level.  $\text{Eu}^{3+}$  is commonly chosen as it possesses individual power states [ ${}^5\text{D}_1/{}^5\text{D}_0$ ], typically considered heat-incorporated discharge states [13], [14]. The occupants for said discharge states adhere to Boltzmann allocation and would be affected through heat level. Phosphor samples incorporated with  $\text{Eu}^{3+}$ , including  $\text{Sr}_2\text{CeO}_4:\text{Eu}^{3+}$ ,  $\text{YNbO}_4:\text{Eu}^{3+}$ , were employed luminescent heat measurement [15]. On the other hand, there are no study that concerns optical heat measurement using  $\text{CaSr}_2(\text{PO}_4)_2:\text{Eu}^{3+}$ .

The creation process for  $\text{CaSr}_2(\text{PO}_4)_2:\text{Eu}^{3+}$  employs the fluid ignition procedure. Following the process, the study will assess the samples' formation, photoluminescence, optical attributes, degradation arch along with Fourier transmute infrared spectroscopy spectrum. Furthermore, for the task of determining the samples' performance for heat measurement as well as solid-state illumination, the study will assess the heat level tracking mechanism for the samples via the fluorescent intenseness proportion for the discharge lines between  ${}^5\text{D}_1$  and  ${}^7\text{F}_1$  as well as between  ${}^5\text{D}_0$  and  ${}^7\text{F}_2$  under heat level range between 323 K and 563 K.

## 2. METHOD

The study employs the ignition procedure for the task of creating  $\text{CaSr}_{(2-2x)}\text{Eu}_x(\text{PO}_4)_2$  in powder form with x value of 0.03. The catalyst included urea as it has superior lowering valence as well as possessing N-N bindings to to assist in the ignition. Uncontaminated ingredients, acquired through sigma Aldrich included calcium nitrate tetrahydrate [ $\text{Ca}(\text{NO}_3)_2 \cdot 4\text{H}_2\text{O}$ ] (99.0%), urea [ $\text{H}_2\text{NCONH}_2$ ] (99.0%), europium nitrate [ $\text{EuNO}_3$ ] (99.9%), strontium nitrate [ $\text{Sr}(\text{NO}_3)_2$ ] (99.9%), and ammonium dihydrogen orthophosphate [ $\text{NH}_4\text{H}_2\text{PO}_4$ ] (99.0%). In the case of  $\text{CaSr}_2(\text{PO}_4)_2$  host, the optimal, static doping content was 3 mol% for task of assessing the luminescence as well as heat measurement for the samples as shown in (1)-(3) [16]–[18].

$$D = \frac{K\lambda}{\beta \cdot \text{Cos}\theta} \quad (1)$$

$$D = \frac{K\lambda}{\beta \cdot \text{Cos}\theta} \quad (2)$$

$$\beta = \frac{K\lambda}{D \cdot \text{Cos}\theta} \quad (3)$$

The natural logarithm will be expressed by (4) and (5).

$$\ln(\beta) = \ln \frac{K\lambda}{D \cdot \text{Cos}\theta} = \ln \frac{K\lambda}{D} + \ln \frac{1}{\text{Cos}\theta} \quad (4)$$

$$\ln\left(\frac{I_0}{I}\right) = \ln(D) - \frac{\Delta E}{kT} \quad (5)$$

$I_0$  and  $I_T$  respectively signify the photoluminescent discharge intenseness for the samples under room temperature and the experimenting temperature. The constant D have no influence on computations. k signifies the Boltzmann constant ( $8.62 \times 10^{-5} \text{ eV} \cdot \text{K}^{-1}$ ). Figure 1 demonstrates the graph for  $\ln [(I_0/I_T)-1]$  with  $1/kT$ , exhibiting one linear dash based on the Arrhenius expression. The dash fitting yields negative result for the arch (-0.257), suggesting superior trigger power as well as superior heat consistency for  $\text{CaSr}_2(\text{PO}_4)_2:\text{Eu}^{3+}$ .

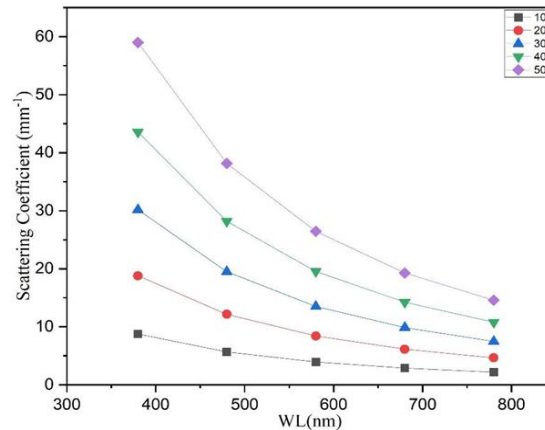


Figure 1. Scattering coefficient and corresponding wavelength

### 3. RESULTS AND DISCUSSION

With the CIE criterion proposed within the twentieth century, acquiring certain hues now involves the hue coordinates  $x$  and  $y$  via key sources. The foundation for exhibition techniques as of today involves creating a merger between red, blue as well as green phosphors for the task of generating a hue from the hue triangle that is established via the hue coordinates from three key sources. Afterwards, we can merge these sources to generate white ray [19]. In general, hue exhibition only requires these sources that are accompanied by appropriate hue coordinates, without the need for the discharge spectrum from the sources. As such, desirable hue generation for discharging exhibitors proves to be simple to realize. It would be highly challenging to generate desirable illumination for universal optical purposes. Due to how our sight reacts illumination, the correlation concerning spectrum and seen hue does not exist. Two lighting devices may yield identical white rays, albeit with disparate discharge spectra. Our sight may lead us to believe that the rays look identical, they would not be the same. The mechanism between scattering coefficient and wavelength is exhibited by Figure 1. The scattering coefficients are at their peaks under roughly 400 nm. As wavelength increases, they dwindle substantially to the bottom under roughly 800 nm, suggesting a reversed correlation. The content is at its peak under 0 wt.%, then almost linearly shrinks under greater particle sizes, reaching its lowest point under 50 wt.%. As wavelength surges, the scattering coefficient is heightened, leading to dispersion for the illumination generated via the blue chip being propagated then transmuted more into rays under bigger wavelengths [20], [21]. Subsequently, the luminescence will be heightened when the blue-ray dispersion within the fore discharge surge with the blue-ray repeating absorptivity as well as rear-dispersion diminished. For the task of acquiring this outcome, the YGA:Ce content must decline when  $\text{SiO}_2$  particle size surges. Subsequently, the CCT disparity will be lessened. The YAG:Ce content's decline associated with particle size of  $\text{SiO}_2$  is displayed by Figure 2. As the particle size surges, the YAG:Ce content diminishes consistently [22].

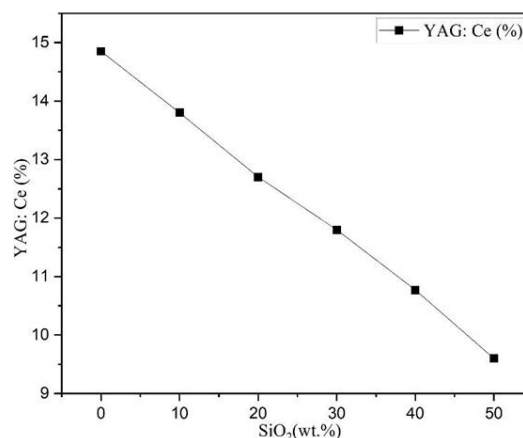


Figure 2. YGA:Ce content correlating with particle size of  $\text{SiO}_2$

Figure 3 showcases CCT interacting with the particle size. With particle sizes of 10, 40 and 0 wt.%, CCT assumes the lowest values of around 3850 K and 3900 K. CCT reaches a greater extent with particle sizes of 20 and 50 wt.%. The particle size of SiO<sub>2</sub> can also influence the hue aberration illustrated by Figure 4. The hue aberration shows noticeable and inconsistent variations with different particle sizes, reaching its peak under 10 wt.% from a median value. Under 30 wt.%, the hue aberration plummets to the bottom. It exhibits significant increase under 40 wt.%, only to plummet again under 50 wt.%. The generated lumen is also altered by particle size of SiO<sub>2</sub> in Figure 5, again showing highly disparate shifts. The lumen shows a great increase as the size reaches 20 wt.%, then witness a sudden sink under 40 wt.%. It then suddenly rises to the top with 50 wt.%. The demonstrated sink could result from the disparity for hue allocation as well as lesser intenseness for blue discharge caused by greater rear-dispersion as well as repeating absorptivity. It is worth noting that under greater particle size, the illumination transmutation between blue and yellow or red-orange will be heightened since the phosphor sheet usually has greater breadth under greater particle size, and as such, the entire spectrum energy deteriorates. This means that under enormous particle size, the transmuted ray may engage in rear-reflection and as a result diminish the luminescent intenseness and yield greater CCT level. 5 wt.% for particle size proves to be an appropriate value in WLED devices to attain superior hue consistency (from lesser hue aberration) as well as superior luminescent intenseness [23].

Besides lumen, the SiO<sub>2</sub> particle size also alters the hue generation in WLED devices. As exhibited by Figures 6 and 7, the particle size of SiO<sub>2</sub> exerts its influence on CRI as well as CQS. For both CRI and CQS, they gradually decline as the particle size surges, albeit in CRI's case, the decline is almost linear. Both parameters are at the peaks under 0 wt.% then through declines, wanes down to the bottom under 50 wt.%. These observed crashes is possibly the result of hue disparity concerning green, blue as well as orange-yellow elements. Under great particle size, the heightened dispersion generates more orange-yellow elements, resulting in said disparity since the ray's discharge hue generally favors the orange-yellow zone. As such, unnecessary dispersion can cause lesser CRI as well as cultural intelligence scale (CQS) [24].

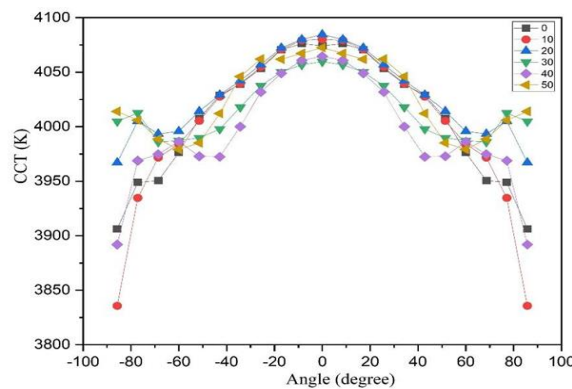


Figure 3. CCT variance based on particle size

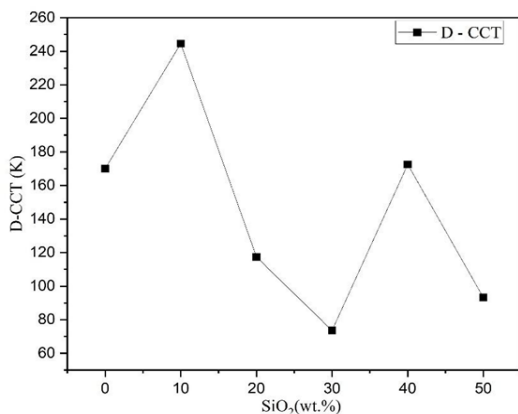


Figure 4. Hue aberration altered by particle size of SiO<sub>2</sub>

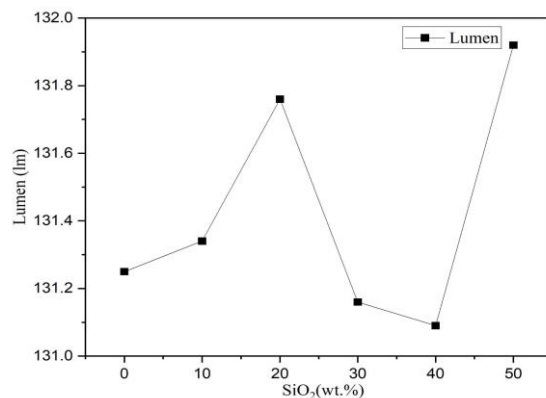


Figure 5. Generated lumen altered by particle size of SiO<sub>2</sub>

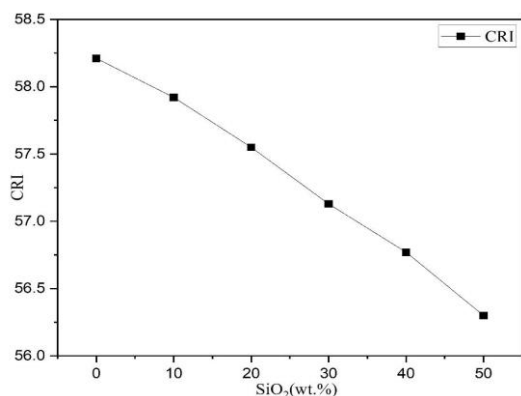


Figure 6. Correlation concerning CRI and particle size of SiO<sub>2</sub>

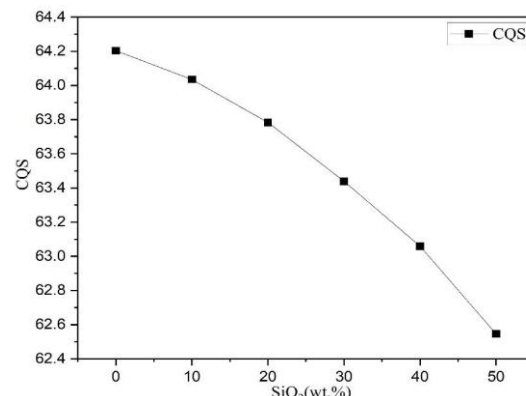


Figure 7. Correlation concerning CQS and particle size of SiO<sub>2</sub>

The task of determining the hue performance for illumination generally involves the use of CRI. This parameter's value range between 1 and 100, which is utilized to gauge how good a ray can recreate the hues in an entity based on the standard of illumination generated by nature. Greater CRI means better hues recreated by the ray. On the other hand, CRI is not particularly reliable if nature's illumination appears to be a black body radiator under 2,700 K. Furthermore, this parameter only takes advantage of eight hues without saturation. As such, when recreating hues with low brightness or saturation, a ray may still yield a significant CRI, whereas a ray with low CRI may still generate vivid hues. Eventually, a different parameter called CQS was proposed to eliminate the shortcomings of CRI and could become the new standard [25], [26]. While CRI takes eight non-saturation hues into account, CQS can assess fifteen hues and thus is able to extend the hue variety in entities with greater precision. Furthermore, this parameter also assesses additional facets: hue distinction as well as individual taste. In case CRI is still considered, it is better to pair CRI with hue temperature that resembles sun ray for the task of assessing the performance of hue generation.

#### 4. CONCLUSION

The study herein concern CaSr<sub>2</sub>(PO<sub>4</sub>)<sub>2</sub>:Eu<sup>3+</sup> phosphor samples created through the ignition procedure. Based on formational assessments, the phosphors were subjected to crystallization, forming pure rhombohedral stage having space group of R3c. When excited under 395 nm, the Eu<sup>3+</sup> discharge lines within the phosphor base exhibited red-orange discharge. The Fourier transmute infrared spectroscopy spectrum validated the existence for orthophosphate anion (PO<sub>4</sub>)<sup>3-</sup> within the samples. When excited under 395 nm, the hue coordinates (0.65, 0.35) remains within the red-orange zone based on CIE graph. On the other hand, we employed the fluorescent intenseness proportion for the task of assessing the samples' performance for luminescent heat measurement. The relative and absolute responsiveness in the samples reached their peak under small heat levels (2.227% K<sup>-1</sup> and 0.0023 K<sup>-1</sup> under 323 K). Judging the outcomes, CaSr<sub>2</sub>(PO<sub>4</sub>)<sub>2</sub>:Eu<sup>3+</sup> can be effectively employed in heat measurement as well as optical field purposes.

#### REFERENCES

- [1] R. Fan, S. Fang, C. Liang, Z. Liang, and H. Zhong, "Controllable one-step doping synthesis for the white-light emission of cesium copper iodide perovskites," *Photonics Research*, vol. 9, no. 5, p. 694, Apr. 2021, doi: 10.1364/prj.415015.
- [2] A. I. Alhassan *et al.*, "Development of high performance green c-plane III-nitride light-emitting diodes," *Optics Express*, vol. 26, no. 5, p. 5591, Feb. 2018, doi: 10.1364/oe.26.005591.
- [3] J.-S. Li, Y. Tang, Z.-T. Li, L.-S. Rao, X.-R. Ding, and B.-H. Yu, "High efficiency solid-liquid hybrid-state quantum dot light-emitting diodes," *Photonics Research*, vol. 6, no. 12, p. 1107, Nov. 2018, doi: 10.1364/prj.6.001107.
- [4] Y. Fei and J. Zhang, "Luminescence properties of KBaYSi<sub>2</sub>O<sub>7</sub>:Ce/Eu-Tb phosphors for multifunctional applications," *Applied Optics*, vol. 58, no. 17, p. 4740, Jun. 2019, doi: 10.1364/ao.58.004740.
- [5] A. Ahmad, A. Kumar, V. Dubey, A. Butola, B. S. Ahluwalia, and D. S. Mehta, "Characterization of color cross-talk of CCD detectors and its influence in multispectral quantitative phase imaging," *Optics Express*, vol. 27, no. 4, p. 4572, Feb. 2019, doi: 10.1364/oe.27.004572.
- [6] F. Jiang *et al.*, "Efficient InGaN-based yellow-light-emitting diodes," *Photonics Research*, vol. 7, no. 2, p. 144, Jan. 2019, doi: 10.1364/prj.7.000144.
- [7] Y. Tang, Z. Li, G. Liang, Z. Li, J. Li, and B. Yu, "Enhancement of luminous efficacy for LED lamps by introducing polyacrylonitrile electrospinning nanofiber film," *Optics Express*, vol. 26, no. 21, p. 27716, Oct. 2018, doi: 10.1364/oe.26.027716.

- [8] Y. J. Park *et al.*, "Development of high luminous efficacy red-emitting phosphor-in-glass for high-power LED lighting systems using our original low Tg and Ts glass," *Optics Letters*, vol. 44, no. 24, p. 6057, Dec. 2019, doi: 10.1364/ol.44.006057.
- [9] L. Xiao, C. Zhang, P. Zhong, and G. He, "Spectral optimization of phosphor-coated white LED for road lighting based on the mesopic limited luminous efficacy and IES color fidelity index," *Applied Optics*, vol. 57, no. 4, p. 931, Feb. 2018, doi: 10.1364/ao.57.000931.
- [10] Q. Zhang, R. Zheng, J. Ding, and W. Wei, "Excellent luminous efficiency and high thermal stability of glass-in-LuAG ceramic for laser-diode-pumped green-emitting phosphor," *Optics Letters*, vol. 43, no. 15, p. 3566, Jul. 2018, doi: 10.1364/ol.43.003566.
- [11] H.-Y. Lee, P. X. Le, and D. Q. A. Nguyen, "Selection of a remote phosphor configuration to enhance the color quality of white LEDs," *Journal of Advanced Engineering and Computation*, vol. 3, no. 4, p. 503, Dec. 2019, doi: 10.25073/jaec.201934.249.
- [12] R. H. Homg, S. Sinha, C. P. Lee, H. A. Feng, C. Y. Chung, and C. W. Tu, "Composite metal substrate for thin film AlGaInP LED applications," *Optics Express*, vol. 27, no. 8, p. A397, Mar. 2019, doi: 10.1364/oe.27.00a397.
- [13] P. Manley, S. Walde, S. Hagedorn, M. Hammerschmidt, S. Burger, and C. Becker, "Nanopatterned sapphire substrates in deep-UV LEDs: is there an optical benefit?," *Optics Express*, vol. 28, no. 3, p. 3619, Jan. 2020, doi: 10.1364/oe.379438.
- [14] Y. Wu *et al.*, "Monolithic integration of MoS<sub>2</sub>-based visible detectors and GaN-based UV detectors," *Photonics Research*, vol. 7, no. 10, p. 1127, Sep. 2019, doi: 10.1364/prj.7.001127.
- [15] E. Xie *et al.*, "High-speed visible light communication based on a III-nitride series-biased micro-LED array," *Journal of Lightwave Technology*, vol. 37, no. 4, pp. 1180–1186, Feb. 2019, doi: 10.1109/JLT.2018.2889380.
- [16] G. S. Archer, "Effect of two different commercially available white light LED fixtures on broiler hatchability and chick quality," *British Poultry Science*, vol. 59, no. 3, pp. 251–255, Feb. 2018, doi: 10.1080/00071668.2018.1436160.
- [17] H. Zhang, Q. Su, and S. Chen, "Recent progress in the device architecture of white quantum-dot light-emitting diodes," *Journal of Information Display*, vol. 20, no. 4, pp. 169–180, Aug. 2019, doi: 10.1080/15980316.2019.1650129.
- [18] J. Chen, B. Fritz, G. Liang, X. Ding, U. Lemmer, and G. Gomard, "Microlens arrays with adjustable aspect ratio fabricated by electrowetting and their application to correlated color temperature tunable light-emitting diodes," *Optics Express*, vol. 27, no. 4, p. A25, Jan. 2019, doi: 10.1364/oe.27.000a25.
- [19] S.-W. Jeon *et al.*, "Optical design of dental light using a remote phosphor light-emitting diode package for improving illumination uniformity," *Applied Optics*, vol. 57, no. 21, p. 5998, Jul. 2018, doi: 10.1364/ao.57.005998.
- [20] T. Hu *et al.*, "Demonstration of color display metasurfaces via immersion lithography on a 12-inch silicon wafer," *Optics Express*, vol. 26, no. 15, p. 19548, Jul. 2018, doi: 10.1364/oe.26.019548.
- [21] S. P. Groth, A. G. Polimeridis, A. Tambova, and J. K. White, "Circulant preconditioning in the volume integral equation method for silicon photonics," *Journal of the Optical Society of America A*, vol. 36, no. 6, p. 1079, May 2019, doi: 10.1364/josaa.36.001079.
- [22] H. S. El-Ghoroury, Y. Nakajima, M. Yeh, E. Liang, C.-L. Chuang, and J. C. Chen, "Color temperature tunable white light based on monolithic color-tunable light emitting diodes," *Optics Express*, vol. 28, no. 2, p. 1206, Jan. 2020, doi: 10.1364/oe.375320.
- [23] P. Zhu, H. Zhu, G. C. Adhikari, and S. Thapa, "Spectral optimization of white light from hybrid metal halide perovskites," *OSA Continuum*, vol. 2, no. 6, p. 1880, May 2019, doi: 10.1364/osac.2.001880.
- [24] D. Chen *et al.*, "Improved electro-optical and photoelectric performance of GaN-based micro-LEDs with an atomic layer deposited AlN passivation layer," *Optics Express*, vol. 29, no. 22, pp. 36559–36566, 2021, doi: 10.1364/OE.439596.
- [25] W. Wang and P. Zhu, "Red photoluminescent Eu<sup>3+</sup>-doped Y<sub>2</sub>O<sub>3</sub> nanospheres for LED-phosphor applications: synthesis and characterization," *Optics Express*, vol. 26, no. 26, pp. 34820–34829, 2018, doi: 10.1364/OE.26.034820.
- [26] K. Chung, J. Sui, T. Sarwar, and P.-C. Ku, "Feasibility study of nanopillar LED array for color-tunable lighting and beyond," *Optics Express*, vol. 27, no. 26, pp. 38229–38235, 2019, doi: 10.1364/OE.382287.

## BIOGRAPHIES OF AUTHORS



**Ho Minh Trung**    received the Ph.D. degree in physics from University of Science, Vietnam National University Ho Chi Minh City, Vietnam. He is working as a lecturer at the Faculty of Basic Sciences, Vinh Long University of Technology Education, Vietnam. His research interests focus on developing the patterned substrate with micro- and nano-scale to apply for physical and chemical devices such as solar cells, OLED, photoanode. He can be contacted at email: trunghm@vlute.edu.vn.



**My Hanh Nguyen Thi**    received a Bachelor of Physics from An Giang University, Viet Nam, Master of Theoretical Physics And Mathematical Physics, Hanoi National University of Education, Viet Nam. Currently. She is a lecturer at the Faculty of Mechanical Engineering, Industrial University of Ho Chi Minh City, Viet Nam. Her research interests are theoretical physics and mathematical physics. She can be contacted at email: nguyenthimyanmarh@iuh.edu.vn.